Chapter 4

Doped Ceria for Solid Oxide Fuel Cells

Shobit Omar

Additional information is available at the end of the chapter

http://dx.doi.org/10.5772/intechopen.79170

Abstract

Lower valent cation-doped CeO_2 materials have attracted remarkable research interest for the electrolyte application in solid oxide fuel cells operating in the intermediate temperature range (500–700°C). At these temperatures, the oxygen-ion conductivity of gadolinium-doped ceria is about an order of magnitude higher than that of yttria-stabilized zirconia. The oxygen-ion diffusion in the cubic fluorite structure of CeO_2 is dependent on several factors such as charge valence and size of dopant cation, doping amount, etc. In the literature, several conductivity trends have been reported as a function of these parameters and are explained by the atomistic computational models. This chapter describes the highlights of the various activities that have been done in this regard to provide insights into the mechanisms underlying the oxygen-ion conduction process in acceptor-doped ceria.

Keywords: bulk ionic conductivity, doped ceria, local defect complexes, defect chemistry, solid oxide fuel cells, electrolyte

1. Introduction

Cerium oxide is the most thoroughly investigated material for the application in solid oxide fuel cells (SOFCs) working in the intermediate-temperature range (500–700°C) [1, 2]. This is because of its pronounced catalytic properties, substantial oxygen-ion conductivity (on doping with lower valent metal oxides) and good phase and thermal stability in the given temperature range. The high catalytic activity in ceria is associated with the presence of Ce^{4+}/Ce^{3+} redox couple which is a key to improve the electrochemical properties of the electrodes. Although this is one area where most of the papers related to ceria have been produced, in this chapter, we restrict our discussion to its usefulness as an electrolyte in SOFCs [3].

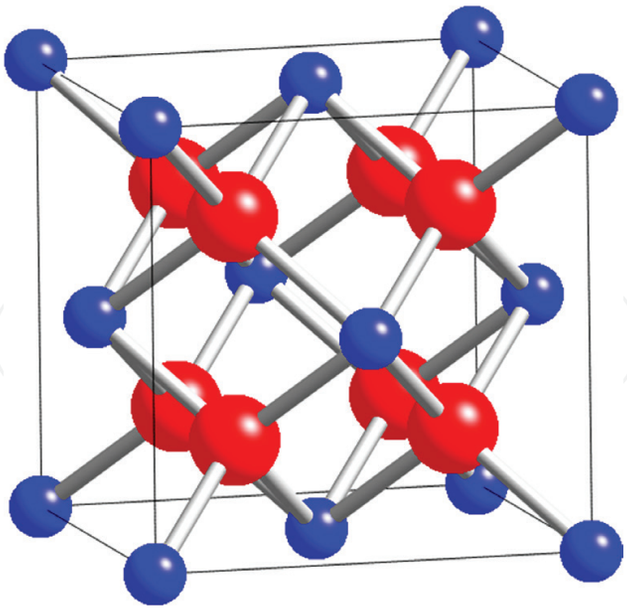

Figure 1. Schematic of a cubic fluorite structure of CeO_2. Ce^{4+} and O^{2-} are shown by blue and red spheres, respectively.

Ceria exhibits a cubic fluorite crystal structure that possesses a relatively large interionic open space facilitating fast oxygen-ion diffusion inside the lattice (shown in **Figure 1**). This open structure is stable from room temperature to its melting point (~2400°C) and allows to accommodate high levels of point defect disorder [4]. Several properties such as ionic conduction, thermoelectric effect, mixed ionic-electronic conductivity, etc., can be altered and tailored by controlling the concentration of these zero-dimensional defects [5]. As a result, the defect engineering in ceria plays a vital role in improving its properties for the electrolyte application.

Oxygen-ion conduction in ceria is mediated through a vacancy diffusion mechanism. In oxidizing atmospheres, the cubic fluorite structure of pure CeO_2 does not have any oxygen vacancy defects. As a result, pure CeO_2 itself is a poor oxygen-ion conductor. The oxygen vacancy defects are introduced into the CeO_2 structure by partially substituting Ce^{4+} with acceptor cations inside the lattice. This can be expressed through the following defect reaction in Kröger-Vink notation.

$$A_2O_3 \xrightarrow{CeO_2} 2A'_{Ce} + 3O_O^x + V_O^{\bullet\bullet} \tag{1}$$

Thus, the impurity center (A'_{Ce}) and oxygen vacancy $(V_O^{\bullet\bullet})$ are the dominant extrinsic ionic defects in trivalent metal oxide doped ceria. Nearly, all oxygen anions vibrate in the region of their tetrahedral sites and under a sufficient driving force, jump from their respective site to the adjacent vacant oxygen-ion site in (100) direction. Though the other conduction pathways are also present, they have a substantially large jump barrier [6]. As a result, the jump distance of oxygen-ion is half the length of the unit cell. During migration from one tetrahedral site to another, oxygen-ion is required to pass through an edge formed by cations shared by the involved tetrahedrons (shown in **Figure 2**).

http://dx.doi.org/10.5772/intechopen.79170

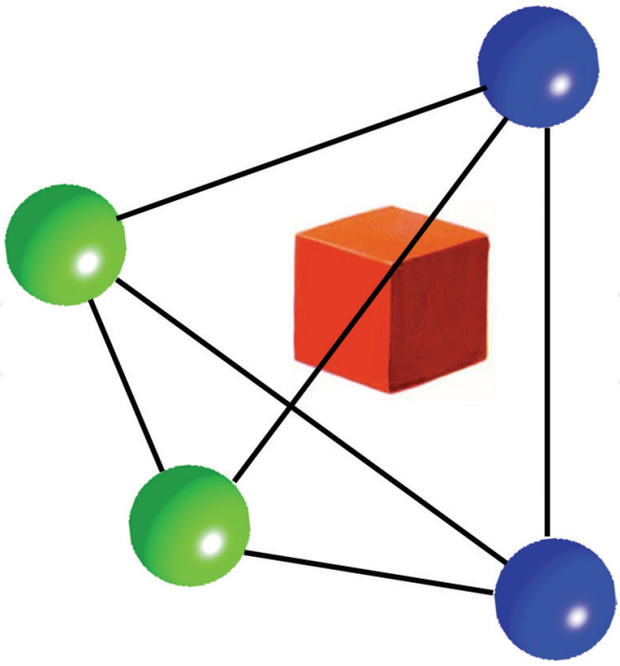

Figure 2. Schematic showing the jump of an oxygen vacancy from one tetrahedral to another through a migration edge. Ce^{4+}, A^{3+} and O^{2-} are shown by blue, green, and red spheres, respectively, while oxygen vacancy is shown by red cube.

For a pure oxygen-ion conductor, oxygen-ion conductivity (σ) can be expressed by,

$$\sigma = \left(1 - \left[V_O^{\bullet\bullet}\right]\right) N_o q_i \mu_i \tag{2}$$

where N_o is the concentration of oxygen sites, $[V_O^{\bullet\bullet}]$ is the fraction of oxygen-ion vacancy and μ_i is the mobility of oxygen-ions with charge denoted as q_i. Several studies have demonstrated that at high temperatures (>700°C) and under the reducing environments (present on the anode side of SOFC device), Ce^{4+} present in ceria tends to reduce to Ce^{3+} leading to the formation of oxygen vacancy and two additional electrons as a charge compensating defect.

$$2\,Ce_{Ce}^{\times} + O_O^{\times} \rightarrow \frac{1}{2}O_2 + V_O^{\bullet\bullet} + 2\,Ce_{Ce}^{/} \tag{3}$$

These electrons are typically localized in the periphery of Ce^{3+}, leading to the formation of small polarons ($Ce_{Ce}^{/}$). These polarons not only break the translation symmetry of crystal but also induce a local lattice distortion around the $Ce_{Ce}^{/}$ site. The migration of polaron results in electronic conduction which contributes a portion of the measured total conductivity in bulk ceria. However, for the solid oxide electrolyte, the electronic conductivity should be kept as low as possible not only to minimize the leakage current which if present decreases the overall cell efficiency, but also to avoid the warping and delamination of electrolyte layer because of the chemical expansion [4]. As a result, the use of doped ceria is restricted to conditions (less than ~700°C, $P_{O_2} > 10^{-18}$ atm) where the electronic conduction is substantially lower than the ionic conduction and thus can be neglected [7].

Oxygen-ion diffusion in doped ceria is a thermally activated process. The temperature dependent behavior of the oxygen-ion conductivity can be expressed through Arrhenius relationship given by,

$$\sigma T = \sigma_o \exp\left(-\frac{E_A}{kT}\right) \tag{4}$$

where σ_o is a pre-exponential factor and E_A is the activation energy of oxygen-ion conduction. The value of E_A is determined from the gradient of the linear-fit of the σ data plotted between logσT versus 1/T. The detailed form of Eq. (4) is given by,

$$\sigma T = \frac{q_V^2}{k}[V_O^{\bullet\bullet}]\left(1-[V_O^{\bullet\bullet}]\right) N_o a^2 \nu_o \exp\left(\frac{\Delta S_m}{k}\right)\exp\left(-\frac{\Delta H_m}{kT}\right) \tag{5}$$

where a is the jump distance of oxygen-ion, ν_o is an appropriate lattice vibration frequency, and ΔS_m and ΔH_m are the change in entropy and enthalpy, respectively, during oxygen-ion diffusion. On comparing Eqs. (4) and (5), it is apparent that the change in enthalpy during oxygen-ion diffusion (ΔH_m) is, in fact, the activation energy (E_A) shown in Eq. (4). Thus, an explicit relationship between the conductivity and temperature is provided in Eq. (5).

It is noteworthy to mention that even though the total conductivity of polycrystalline samples is influenced by the conductivity inside the grains and grain boundaries, in this chapter, we only refer to the grain (bulk) conductivity which occurs by oxygen-ion jump through the regular lattice and is not affected by the microstructural characteristics of the sample. Thus, the bulk ionic conduction is the inherent property of the doped material [8]. On the other hand, the conduction in grain boundaries is dependent on several factors such as impurity segregation, space-charge region, etc. [9]. Both the bulk and grain boundary conductivity can be estimated by acquiring an impedance spectrum over a frequency range (typically 10 MHz to 0.01 Hz) on the polycrystalline sample [10]. As grain boundaries show higher capacitance value (in the range from 10^{-8} to 10^{-11} F) compared to the bulk region (~ 10^{-12} F), two distinct arcs are typically observed associated with these phenomena [10]. On fitting the impedance data using an analog equivalent electric circuit, the resistance offered by bulk and grain boundary regions is estimated which can be then be used in determining the corresponding conductivities.

The bulk conductivity has a significant dependence on the concentration of oxygen vacancy which is controlled by the doping amount according to $2[A_{Ce}^{\prime}] = [V_O^{\bullet\bullet}]$ in A_2O_3-doped CeO_2. It can be observed from Eq. (5) that the conductivity would likely to follow a parabolic behavior as a function of oxygen vacancy concentration and reaches its maximum value when half of the oxygen sublattice is unoccupied. From several investigations on fluorite-structured oxides (including ceria), it has been found that even though conductivity exhibits maxima when plotted against the dopant concentration, the maximum in conductivity appears at significantly lower dopant fractions (less than 0.4) [11–13]. **Figure 3** shows the bulk conductivity of $Sm_{x/2}Nd_{x/2}Ce_{1-x}O_{2-x/2}$ as a function of doping amount (x) at various temperatures [8]. At 550°C, the maximum in conductivity is found at x = 0.15. On lowering the temperature, the doping fraction leading to the maximum in conductivity (x_{max}) shifts toward the lower value. Thus, the conductivity data obtained at low temperatures results in low x_{max}, while the high-temperature data will possess a high value of x_{max} [6]. Further, the x_{max} value is also dependent on the charge valence and size of acceptor dopant used to generate oxygen vacancies in ceria. This is attributed to the formation of local defect complexes which are discussed in the later section.

http://dx.doi.org/10.5772/intechopen.79170

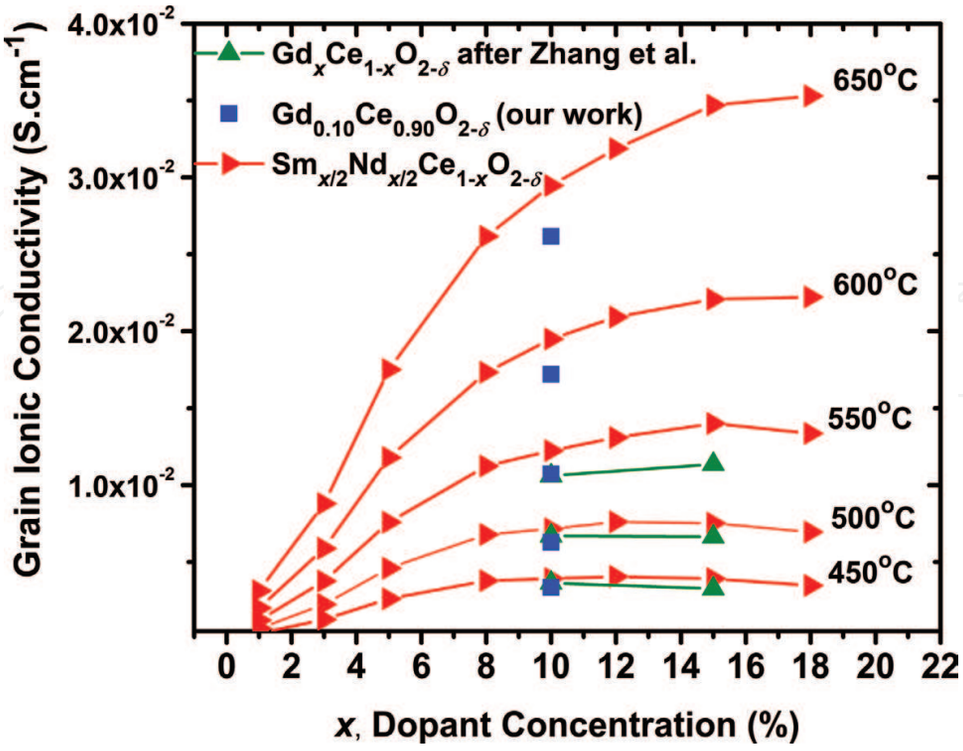

Figure 3. Bulk ionic conductivity is plotted against the dopant concentration (x) in $Sm_{x/2}Nd_{x/2}Ce_{1-x}O_{2-\delta}$ and $Gd_xCe_{1-x}O_{2-\delta}$ [8, 14].

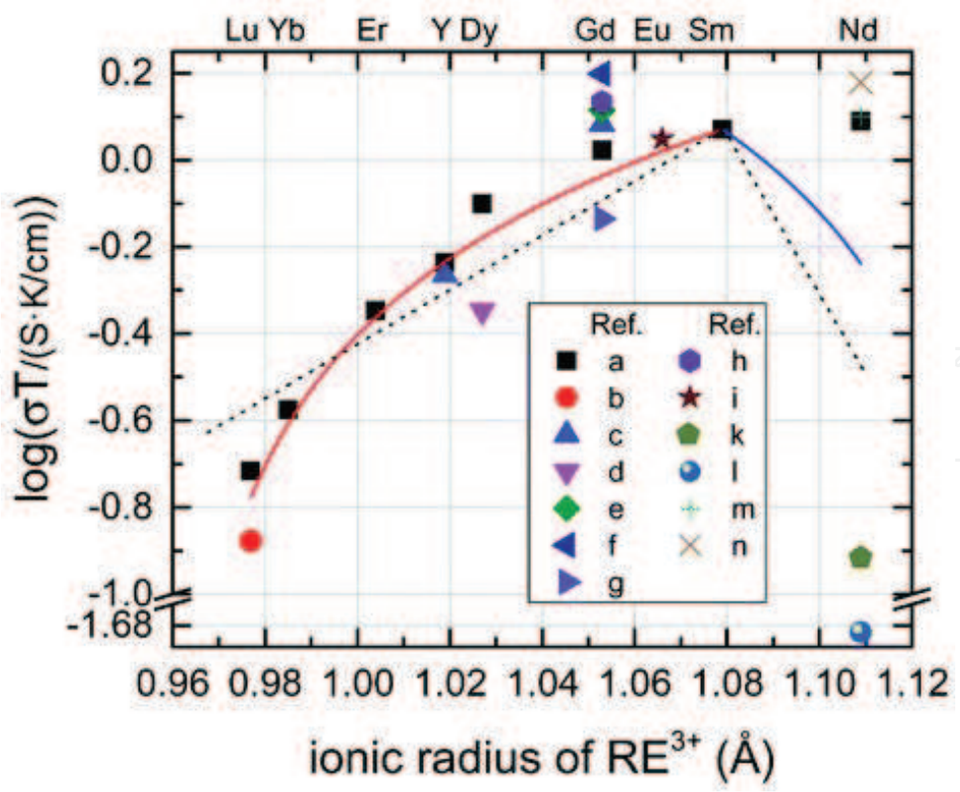

Figure 4. Bulk ionic conductivity of $A_xCe_{1-x}O_{2-x/2}$ (with $x = 0.1$) at 400°C plotted against the radius of dopant cation. The conductivity data are taken according to references a [15], b [23], c [14], d [24], e [25], f [26], g [27], h [28], i [29], k [30], l [31], m [32] and n [33]. The lines show a linear relationship between the ionic radius and the conductivity (solid lines) or the logarithm of the conductivity (dashed lines) [6].

Besides the doping amount, the physical properties of dopant cations also influence the bulk conductivity of ceria. Numerous investigations have been performed to understand these correlations in doped ceria systems [1, 15–19]. **Figure 4** depicts the dependence of ionic conductivity in $A_{0.10}Ce_{0.90}O_{1.95}$ on the ionic size of the trivalent dopant cation (A^{3+}) at 600°C. While the work performed by Omar et al. [15] showed a continuous increase in the bulk conductivity with the increase in ionic size, others [17, 20–22] reported a conductivity maximum around Gd^{3+} and Sm^{3+}. It is interesting to note that the maximum in conductivity observed around these cations is independent of dopant concentration [6]. In the literature, several empirical, semi-empirical and atomistic models have been reported to clarify this and elucidate the effect of doping amount and the dopant-type on the conductivity. This chapter reviews some of these models to provide insights into the mechanisms underlying the oxygen-ion conduction process in doped ceria.

2. Formation of local defect complexes

Whenever charged point defects (A'_{Ce}) are incorporated into the crystal structure, to maintain electroneutrality, defects possessing opposite charges must be created. These oppositely charged defects strongly interact with each other because of electrostatic attraction. Further, the elastic interactions also exist to relax the local stresses surrounding these defects. For example, an oversized substitutional impurity cation may attract an open space of vacancy. This leads to the formation of local defect complexes such as $(A'_{Ce} - V_O^{\bullet\bullet} - A'_{Ce})$ and $(A'_{Ce} - V_O^{\bullet\bullet})^{\bullet}$. These defect complexes trap the oxygen vacancies and effectively reduce the number of mobile oxygen-ions. In most literature, it is commonly accepted that the primary reason for the significant decrease in ionic conductivity of doped ceria at higher dopant content is essentially because of the formation of local defect complexes.

Figure 5 depicts a case where $V_O^{\bullet\bullet}$ defect is trapped in a tetrahedral site of the fluorite structure surrounded by oppositely charged dopant cations and neutral host cations. There are several experimental studies which support the formation of local defect structures. Extended X-ray absorption

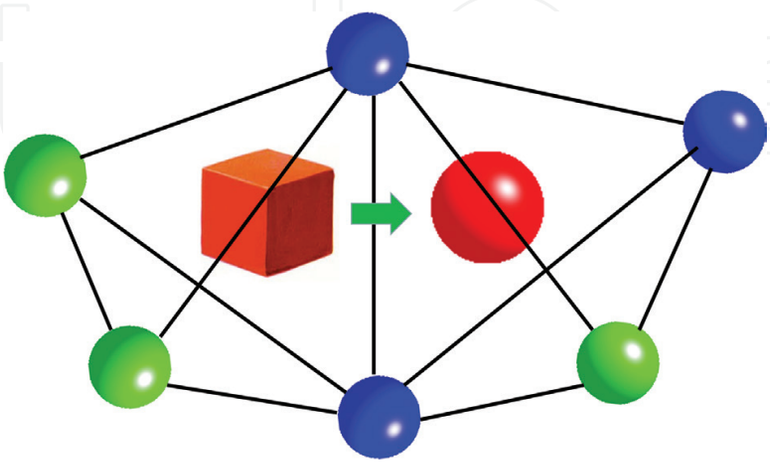

Figure 5. Oxygen vacancy defect trapped inside the tetrahedral void to form local defect complex. Ce^{4+}, A^{3+} and O^{2-} are shown by blue, green, and red spheres, respectively, while oxygen vacancy is shown by red cube.

fine structures (EXAFS) have been extensively utilized to study the local structures around the cations and anions in lower-valent cation-doped ceria [34–36]. In case of $Gd_xCe_{1-x}O_{2-x/2}$, the addition of Gd^{3+} leads to a decrease in the interatomic distance Gd-O which is attributed to the formation of the defect complexes with two Gd^{3+} and one oxygen vacancy [37]. The formation of local defect structure is also evident in the nuclear magnetic resonance study where the average coordination number is estimated for cations in Y^{3+}- and Sc^{3+}-doped CeO_2 [38]. The tendency of oxygen vacancies to preferentially associate with Sc^{3+} was found to be stronger than with Y^{3+} in these systems.

The binding energy associated with the local defect structures is mainly dependent on the electrostatic attraction of the defects caused by the effective charges in the lattice. Further, it also includes terms due to the relaxation of the lattice around the defect which depends on the polarizability and the size of dopant cation. Several groups have found a difference in the magnitudes of E_A when measured in the high- and low-temperature regimes [14, 39]. Typically, the activation energy value estimated in a low-temperature regime is higher than that in the high-temperature region. In a few investigations, a kink is noticed around 350–600°C in the Arrhenius plot of the measured ionic conductivity [14]. Nevertheless, there are several other studies where instead of a sharp, a gradual change in slope with temperature is reported [8, 40]. It has been argued that in a low-temperature regime, most of the oxygen vacancies are bound to various traps to form local defect complexes [41]. However, at higher temperatures, the thermal vibrations of the local defect structures become dominant. At a certain temperature, the thermal energy overcomes the binding energy of these local defect complexes, and the majority of oxygen vacancy defects are set free to migrate from one site to another. Thus, the oxygen vacancies require only migration (ΔH_m) to cross the energy barrier at higher temperatures. As a result, in the low-temperature region, the total E_A is composed of ΔH_m and association enthalpy (ΔH_a), whereas in the high-temperature region, the measured E_A is only because of migration enthalpy of oxygen-ions.

In the literature, several methods have been used to determine the association enthalpy. Omar et al. [42] have taken a difference in the magnitudes of E_A obtained in the high- and low-temperature regimes and reported the association enthalpy in $Sm_{x/2}Nd_{x/2}Ce_{1-x}O_{2-x/2}$ in the range

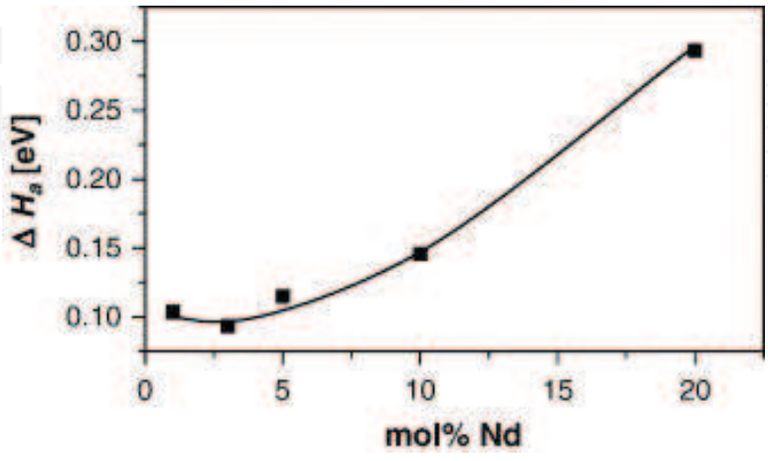

Figure 6. Association enthalpy (ΔH_a) is plotted against the Nd^{3+} doping amount in $Ce_{1-x}Nd_xO_{2-x/2}$. For the calculation of ΔH_a, the minimum value of the E_A measured in the low-temperature range (i.e., below 350°C) has been assumed to be equal to the enthalpy of migration [32].

of 0.02–0.05 eV [42]. Nowick et al. [43] obtained the association enthalpy by estimating the migration enthalpy in pure CeO_2 to be 0.67 eV. Stephen and Kilner [32] have taken the minimum value of E_A measured in the low-temperature regime in $Nd_xCe_{1-x}O_{2-x/2}$ as a migration enthalpy. The association enthalpy initially decreases and then increases after reaching a minimum value at $x = 0.03$ (shown in **Figure 6**) [32]. The increase in association enthalpy is attributed to the development of deep vacancy association. A similar trend in association enthalpy is also observed for other dopant cations such as Y^{3+}, Gd^{3+} and Sm^{3+} and so on [11, 14, 44].

3. Elastic lattice strain

The amount of local defect structures increases with the incorporation of oxygen vacancies inside the lattice. For achieving high oxygen-ion conductivity, the association of defects needs to be minimized. Kilner and Brook [45] stated that the oxygen-ion conductivity in doped CeO_2 could be enhanced if the elastic strain present in the lattice is lowered. Kim [46] partially replaced acceptor cations in fluorite-structured MO_2 (where M is a tetravalent cation) and studied the change in lattice parameter of the host oxides. By performing multiple regression analysis, an empirical model was developed that can predict the elastic strain in doped ceria systems for any given dopant cation. This model takes into consideration the size mismatch and difference in charge valence between the dopant and host cations and the dopant concentration. Further, Kim [46] proposed the concept of critical ionic radius (r_c) which was described as the ionic radius of a cation which on doping leads to a negligible distortion in the host fluorite lattice. For the trivalent dopant cation and host ceria, the value of r_c was estimated to be 1.038 Å. Based on Kilner and Brook's prediction, the cation with the ionic radius of r_c is the optimal dopant that can lead to the maximum oxygen-ion conductivity in CeO_2 [45]. As a result, the oxygen-ion conductivity in doped CeO_2 depend upon the ($|r_d - r_c|$) value, where r_d is the ionic radius of dopant. The lower the $|r_d - r_c|$ value for a particular dopant, the higher the ionic conductivity for that system is expected to be. Kim [46] argued that the highest ionic conductivity is observed around Gd^{3+} (see **Figure 4**) as r_c value is close to the ionic radius of Gd^{3+} ($r_{Gd,VIII}{}^{3+} = 1.053$ Å).

In a similar study, Hong and Virkar [47] calculated the r_c value to be 1.024 Å using a simple analytical model that can also predict the elastic lattice strain present in doped CeO_2. In this model, the oxygen vacancy is treated as one of the chemical species whose size remains constant irrespective of the size and concentration of dopant cation.

To examine the validity of minimum strain's hypothesis, Omar et al. [23] have carried out the experimental studies using a novel co-doping strategy in ceria. A co-dopant pair of Lu^{3+} and Nd^{3+} were chosen and added in a ratio such that the weighted average dopant ionic radius of co-dopants matches the magnitude of r_c. Using this approach, it is expected that, on average, the positive elastic strain because of larger dopant cation (i.e., Nd^{3+}) is compensated by the negative elastic strain caused by the smaller dopant cation (i.e., Lu^{3+}). This, as a result, prevents any distortion in fluorite lattice that is usually present in singly doped ceria systems. On calculating the lattice parameter, almost negligible elastic lattice strain was seen in these systems (see **Figure 7**). However, the ionic conductivity in Lu^{3+} and Nd^{3+} co-doped

http://dx.doi.org/10.5772/intechopen.79170

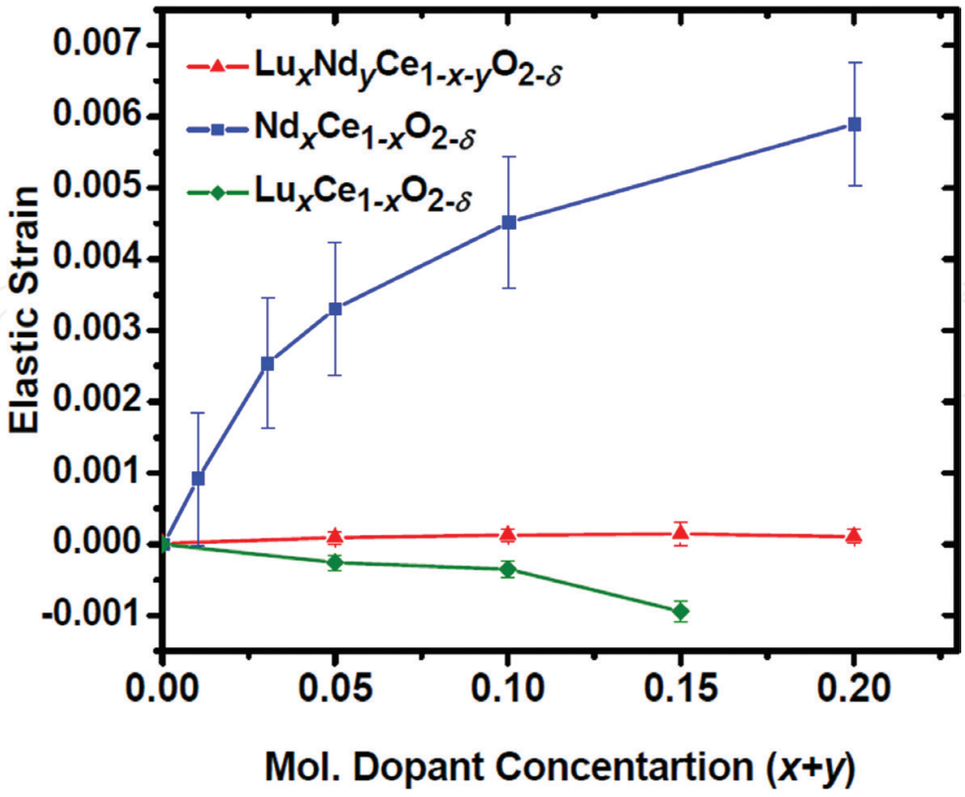

Figure 7. Elastic strain is plotted against the dopant concentration [23]. Data for $Nd_xCe_{1-x}O_{2-\delta}$ were taken after Stephens et al. [32].

CeO_2 system was found to be lower than that of Gd^{3+}-doped CeO_2 [23]. Thus, even though the co-doped CeO_2 system exhibits minimal elastic strain, its oxygen-ion conductivity remains inferior to that of Gd^{3+}-doped CeO_2.

On plotting the activation energy for oxygen-ion diffusion in trivalent cation-doped CeO_2, it has been found that the minimum value for activation energy occurs for Sm^{3+} which possesses a much larger ionic radius than the r_c value [15]. Thus, both co-doping results and the obtained activation energy values do not support the hypothesis given by Kilner and Brook [45] that the highest oxygen-ion conductivity is obtained in the system having a negligible elastic lattice strain. However, it is noteworthy to mention that all the r_c values reported in the literature are derived from the empirical relationships which are based on the lattice expansion data acquired at room temperature. As the oxygen-ion conductivity of doped CeO_2 materials is usually measured between 400°C and 700°C, there is a possibility that the r_c value increases with the increasing temperature. Omar et al. [15] tested this hypothesis by measuring the lattice distortion for various doped CeO_2 systems (with 10 mol.% dopant concentration) at higher temperatures. The r_c value was then determined, where the lattice parameter mismatch between doped and pure CeO_2 becomes zero (see **Figure 8**). It was noticed that the r_c value decreases with the increase in temperature and does not follow the conductivity trend. The obtained results clearly indicate that the oxygen-ion conductivity is not solely dependent on elastic strain, and therefore, a structure-conductivity relationship based on the critical ionic radius concept is insufficient to describe the conduction behavior in doped ceria.

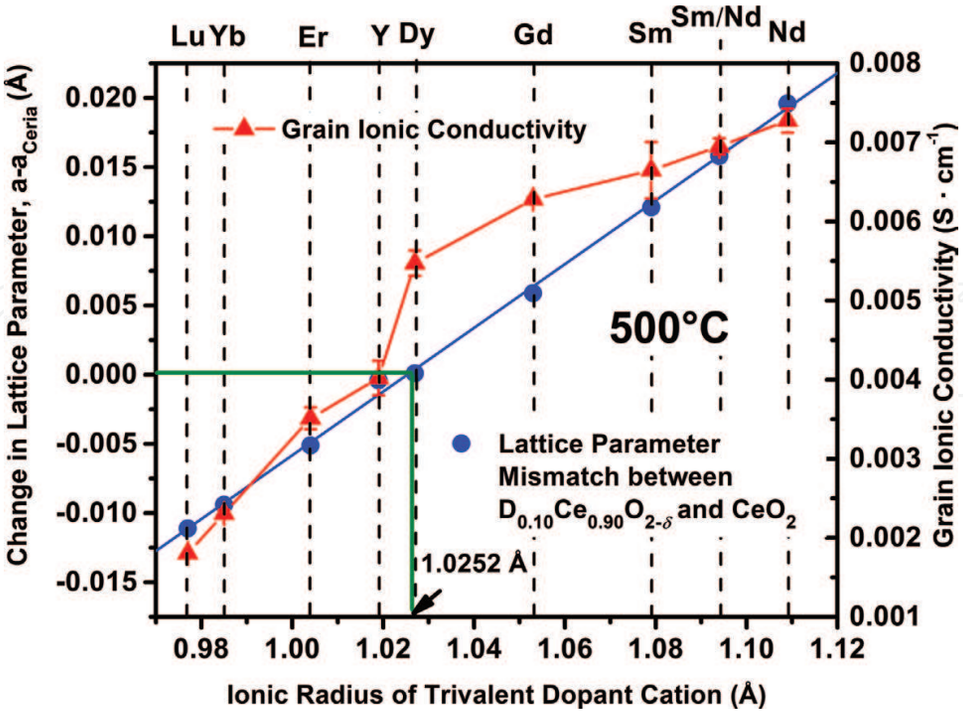

Figure 8. Lattice parameter mismatch between $A_{0.10}Ce_{0.90}O_{2-\delta}$ and CeO_2 is plotted against the ionic radius of dopant cation (A^{3+}) at 500°C. The grain (bulk) oxygen-ion conductivity of $A_{0.10}Ce_{0.90}O_{2-\delta}$ at 500°C is also shown [15].

4. Dopant cation-oxygen vacancy interaction energetic

In the past, multiple atomistic computer simulation techniques have been used to study the interaction energetic involved between the cations and oxygen vacancies in acceptor cation-doped CeO_2. Butler et al. [48] reported that the ionic radius of dopant has a major influence on the stability of defect complexes. Minervini et al. [49] studied the binding energy of an oxygen vacancy with dopant cation using the energy minimization techniques. It was found that the oxygen vacancies prefer to reside in the first neighboring sites of small dopant cations and in the second neighboring sites of large dopant cations. For Gd^{3+} dopant cation, the oxygen vacancy shows similar preference to reside in first and second neighboring sites. Moreover, the binding energy was also estimated to be lowest in Gd^{3+}-doped CeO_2. Although these theoretical studies show a close match with the experimental results, they are based on empirical atomistic models.

Andersson et al. [16] performed the quantum mechanical calculations within the density functional theory (DFT) formalism in trivalent cation-doped CeO_2. Both electrostatic and elastic interaction energies between the dopant cation and oxygen vacancy located in nearest neighbor (NN) site and in the next to nearest neighbor (NNN) site (of dopant cation) were predicted using the *ab-initio* calculations. It was found that for Pm^{3+} dopant cation, the total interaction energy values are similar for both the configurations (shown in **Figure 9**). As a result, the Pm^{3+}-doped CeO_2 system contains the maximum number of oxygen sites with equi-interaction energy inside the host lattice. There will be no site preference for oxygen vacancies

http://dx.doi.org/10.5772/intechopen.79170

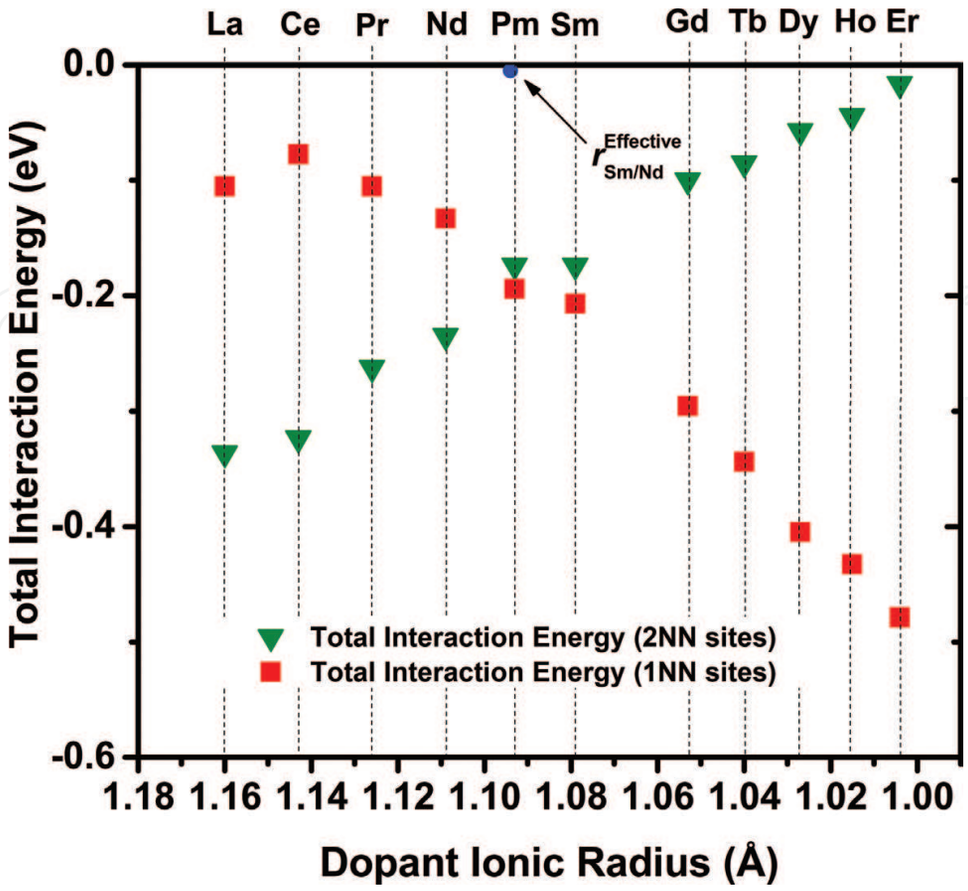

Figure 9. Total interaction energy between dopant cation and oxygen vacancy sitting in nearest neighbor (NN) and next to nearest neighbor (NNN) site (of dopant cations) for rare- earth dopant cations. The negative numbers imply attractive interactions. The $r^{Effective}_{Sm/Nd}$ is the weighted average ionic radius of Sm^{3+}/Nd^{3+}. The figure is modified after Andersson et al. [16].

which leads to minimal deep traps inside the doped ceria lattice. Thus, Pm^{3+}-doped CeO_2 was predicted to exhibit higher oxygen-ion conductivity than any other acceptor-doped ceria materials.

Unfortunately, Pm is a radioactive element and cannot be used as a dopant in ceria. The best dopant should be having an effective atomic number around Pm^{3+} (61) with an ionic radius of 1.093 Å. According to Andersson et al. [16], a co-doping approach, with Sm^{3+} and Nd^{3+} as co-dopants, provides an experimental scenario for examining the validity of this hypothesis. Omar et al. [8, 42] have studied the influence of co-doping Sm^{3+} and Nd^{3+} on the oxygen-ion conductivity of CeO_2. Sm^{3+} and Nd^{3+} were added in an equal ratio to obtain the effective atomic number of Pm^{3+}, that is, 61. By doing so, similar total interactions between the dopant cations and oxygen vacancies sitting in NN and NNN sites (of dopant cations) are expected, which may lead to enhancement in the oxygen-ion conductivity. It was reported that for compositions containing 10 mol.% of dopant, Sm^{3+} and Nd^{3+}-doped ceria exhibits 14% higher grain ionic conductivity than that of $Gd_{0.10}Ce_{0.90}O_{2.95}$ at 550°C, in air (shown in **Figure 3**). The obtained high conductivity of co-doped samples validates the density functional theory prediction about Pm^{3+} to be the best dopant cation for achieving high oxygen-ion conductivity in CeO_2.

5. Migration enthalpy in the local environment

Although several investigations have shown the formation of local defect structures in doped ceria systems, only a few models exist which describe the doping fraction at which they start appearing and directly influencing the conductivity. Also, in several experimental investigations, the observed trend in macroscopic migration enthalpy is attributed to the microscopic level association between dopant cation and oxygen vacancies without a thorough understanding of underlying atomistic level mechanisms. In earlier studies, the local defect structures are considered as one of the chemical species whose concentration is described using the equilibrium thermodynamics [1, 39]. However, this approach does not take into account the interactions between the local defect structures, especially at higher doping concentrations (>10 mol.% A_2O_3).

Multiple atomistic simulations studies have been performed to comprehend the relationships between the macroscopic conductivity and the migration in various local environments. In one of the earlier theoretical studies, Murray et al. [50] used Kinetic Monte Carlo (KMC) simulations to consider the migration enthalpy in the local environment to estimate the oxygen-ion conductivity as a function of doping level. It was reported that at higher doping concentration, oxygen vacancies tend to reside next to dopants, and thus do not contribute toward ionic conduction.

In a similar investigation, Nakayama et al. [51] used *ab-initio* density functional theory calculations to identify two key relationships that govern the oxygen-ion migration in rare-earth cation-doped ceria. First, the lowering of migration energy barrier by doping with a smaller trivalent cation would be accompanied by trapping of an oxygen vacancy at the nearest neighboring sites of the dopant. Second, doping with a larger trivalent cation increases the energy barrier but decreases the trapping effect of oxygen vacancies. Thus, the relative magnitude of these two effects is dependent on the size of dopant cation which in turn decides the magnitude of oxygen-ion conductivity.

In recent work by Koettgen et al. [6], the oxygen-ion conductivity was calculated as a function of the doping amount by combining *ab-initio* density functional theory and Kinetic Monte Carlo simulations. A model was developed that can estimate migration energies for all the possible jump configurations present in rare-earth-doped CeO_2 system. Migration energies were analyzed for energy contributions that are either energetically symmetric for both migration directions, that is, forward and backward jumps or energetically asymmetric for the forward and backward directions. If the presence of dopant changes the migration energy identically in both the backward and forward directions, the energy contribution, in this case, is referred to as blocking. On the other hand, if the migration energy is different for forward and backward jumps, the energy contribution is referred to as trapping.

Figure 10 shows the schematic of trapping and blocking effects. The energy of the system as a function of a reaction coordinate for the corresponding configuration is also shown. It was demonstrated that both these effects have an impact on the observed ionic conductivity. While blocking effect determines the doping fraction at which the maximum in conductivity is observed, it is the trapping effect which limits the maximum ionic conductivity value.

http://dx.doi.org/10.5772/intechopen.79170

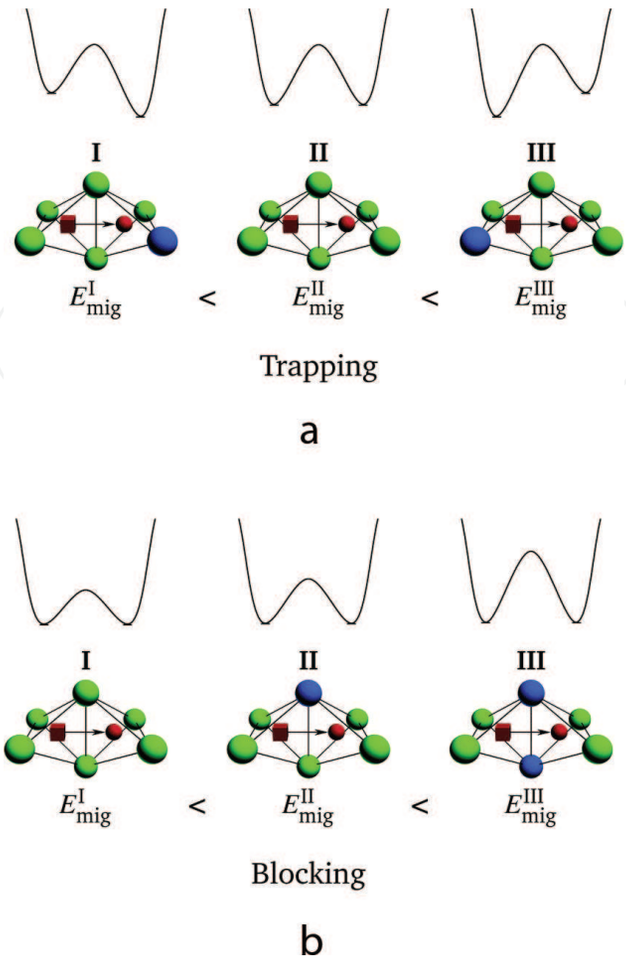

Figure 10. The energy of the system as a function of the reaction coordinate for the configuration change that is shown below in rare-earth-doped ceria. In trapping effect, migration enthalpy increases if the oxygen-ion jump weakens the association between the oxygen vacancies and the dopants. In case of blocking effect, the migration energy increases for an increasing number of large dopants at the migration edge: cerium ions (green), rare-earth ions (blue), oxygen ions (red spheres), and oxygen vacancies (red boxes) [6].

Thus, this study clarifies that the optimal doping concentration to achieve the maximum ionic conductivity cannot be predicted only by trapping effect (association between dopant cation and oxygen vacancies) which is commonly assumed in the literature.

6. Summary and conclusion

This chapter reviews some of the highlights of investigations performed on lower-valent cation-doped ceria materials which have been considered strong candidates for the electrolyte application in SOFCs operating at the intermediate-temperature range. Some of the basic characteristics of doped ceria relating to its high oxygen-ion conductivity are discussed. The maximum in conductivity observed by adding a large amount of lower-valent dopant cation is explained on the basis of formation of local defect structures. The extent of formation of these local defect structures cannot be lowered by just minimizing the elastic lattice distortion. It has been emphasized

that the concept of critical ionic radius alone cannot explain the maximum oxygen-ion conductivity observed in Pm^{3+}-doped CeO_2 as found by the first-principles density functional theory calculations. Particular attention has been given to a more recent atomistic simulations study on rare-earth-doped ceria which calculates the migration energies for all the possible jump configurations that may present in rare-earth-doped CeO_2. This study explains the importance of the shape of migration energy barrier and its impact on the ionic conductivity.

Acknowledgements

Author would like to acknowledge IIT Kanpur for supporting in writing this chapter.

Author details

Shobit Omar

Address all correspondence to: somar@iitk.ac.in

Department of Materials Science and Engineering, Indian Institute of Technology Kanpur, Kanpur, Uttar Pradesh, India

References

[1] Inaba H, Tagawa H. Ceria-based solid electrolytes - review. Solid State Ionics. 1996;**83**:1-16

[2] Steele BCH. Appraisal of $Ce_{1-y}Gd_yO_{2-y/2}$ electrolytes for IT-SOFC operation at 500° C. Solid State Ionics. 2000;**129**:95-110

[3] Mogensen M, Sammes NM, Tompsett GA. Physical, chemical and electrochemical properties of pure and doped ceria. Solid State Ionics. 2000;**129**:63-94

[4] Omar S, Nino JC. Consistency in the chemical expansion of fluorites: A thermal revision of the doped ceria. Acta Materialia. 2013;**61**:5406-5413

[5] Tuller HL, Bishop SR. Tailoring material properties through defect engineering. Chemistry Letters. 2010;**39**:1226-1231

[6] Koettgen J, Grieshammer S, Hein P, Grope BOH, Nakayama M, Martin M. Understanding the ionic conductivity maximum in doped ceria: Trapping and blocking. Physical Chemistry Chemical Physics. 2018;**20**:14291-14321

[7] Zhu H, Ricote S, Coors WG, Chatzichristodoulou C, Kee RJ. Equilibrium and transient conductivity for gadolium-doped ceria under large perturbations: II. Modeling. Solid State Ionics. 2014;**268**:198-207

[8] Omar S, Wachsman ED, Nino JC. Higher ionic conductive ceria based electrolytes for SOFCs. Applied Physics Letters. 2007;**91**:144106

[9] Guo X, Waser R. Electrical properties of the grain boundaries of oxygen ion conductors: Acceptor-doped zirconia and ceria. Progress in Materials Science. 2006;**51**:151-210

[10] Irvine JTS, Sinclair DC, West AR. Electroceramics: Characterization by impedance spectroscopy. Advanced Materials. 1990;**2**:132-138

[11] Wang DY, Park DS, Griffith J, Nowick AS. Oxygen-ion conductivity and defect interactions in Yttria-doped ceria. Solid State Ionics. 1981;**2**:95-105

[12] Yahiro H, Eguchi Y, Eguchi K, Arai H. Oxygen ion conductivity of the ceria-samarium oxide system with fluorite structure. Journal of Applied Electrochemistry. 1988;**18**:527-531

[13] Yahiro H, Ohuchi T, Eguchi K, Arai H. Electrical-properties and microstructure in the system ceria alkaline-earth oxide. Journal of Materials Science. 1988;**23**:1036-1041

[14] Zhang TS, Ma J, Kong LB, Chan SH, Kilner JA. Aging behavior and ionic conductivity of ceria-based ceramics: A comparative study. Solid State Ionics. 2004;**170**:209-217

[15] Omar S, Wachsman ED, Jones JL, Nino JC. Crystal structure-ionic conductivity relationships in doped ceria systems. Journal of the American Ceramic Society. 2009;**92**:2674-2681

[16] Andersson DA, Simak SI, Skorodumova NV, Abrikosov IA, Johansson B. Optimization of ionic conductivity in doped ceria. Proceedings of the National Academy of Sciences of the United States of America. 2006;**103**:3518

[17] Balazs GB, Glass RS. AC-impedance studies of rare-earth-oxide doped ceria. Solid State Ionics. 1995;**76**:155-162

[18] Butler V, Catlow CRA, Fender BEF, Harding JH. Dopant ion radius and ionic-conductivity in cerium dioxide. Solid State Ionics. 1983;**8**:109-113

[19] Gerhardt-Anderson R, Nowick AS. Ionic conductivity of CeO_2 with trivalent dopants of different ionic radii. Solid State Ionics. 1981;**5**:547-550

[20] Perez-Coll D, Marrero-Lopez D, Nunez P, Pinol S, Frade JR. Grain boundary conductivity of $Ce_{0.8}Ln_{0.2}O_{2-d}$ ceramics (Ln = Y, La, Gd, Sm) with and without co-doping. Electrochimica Acta. 2006;**51**:6463-6469

[21] Zając W, Molenda J. Electrical conductivity of doubly doped ceria. Solid State Ionics. 2008;**179**:154-158

[22] Mogensen M, Lindegaard T, Hansen UR, Mogensen G. Physical properties of mixed conductor solid oxide fuel cell anodes of doped CeO2. Journal of the Electrochemical Society. 1994;**141**:2122-2128

[23] Omar S, Wachsman ED, Nino JC. A co-doping approach towards enhanced ionic conductivity in fluorite-based electrolytes. Solid State Ionics. 2006;**177**:3199-3203

[24] Sánchez-Bautista C, Dos santos-García AJ, Peña-Martínez J, Canales-Vázquez J. The grain boundary effect on dysprosium doped ceria. Solid State Ionics. 2010;**181**:1665-1673

[25] Tianshu Z, Hing P, Huang H, Kilner J. Ionic conductivity in the CeO_2–Gd_2O_3 system ($0.05 \leq Gd/Ce \leq 0.4$) prepared by oxalate coprecipitation. Solid State Ionics. 2002;**148**:567-573

[26] Fuentes RO, Baker RT. Structural, morphological and electrical properties of Gd0.1Ce0.9O1.95 prepared by a citrate complexation method. Journal of Power Sources. 2009;**186**:268-277

[27] Keqin H, Man F, Goodenough JB. Synthesis and electrical properties of dense Ce0.9Gd0.1O1.95 ceramics. Journal of the American Ceramic Society. 1998;**81**:357-362

[28] Reddy KR, Karan K. Sinterability, Mechanical, Microstructural, and electrical properties of gadolinium-doped ceria electrolyte for low-temperature solid. Journal of Electroceramics. 2005;**15**:45-56

[29] Cioateră N, Pârvulescu V, Rolle A, Vannier RN. Effect of strontium addition on europium-doped ceria properties. Solid State Ionics. 2009;**180**:681-687

[30] Li LP, Lin XM, Li GS, Inomata H. Solid solubility and transport properties of $Ce_{1-x}Nd_xO_{2-d}$ Nanocrystalline solid solutions by a sol-gel route. Journal of Materials Research. 2001;**16**:3207-3213

[31] Aneflous L, Musso JA, Villain S, Gavarri JR, Benyaich H. Effects of temperature and Nd composition on non-linear transport properties in substituted $Ce_{1-x}Nd_xO_{2-\delta}$ cerium dioxides. Journal of Solid State Chemistry. 2004;**177**:856-865

[32] Stephens IEL, Kilner JA. Ionic conductivity of $Ce_{1-x}Nd_xO_{2-x/2}$. Solid State Ionics. 2006;**177**:669-676

[33] Zhu JX, Zhou DF, Guo SR, Ye JF, Hao XF, Cao XQ, Meng J. Grain boundary conductivity of high purity neodymium-doped ceria nanosystem with and without the doping of molybdenum oxide. Journal of Power Sources. 2007;**174**:114-123

[34] Yamazaki S, Matsui T, Sato T, Arita Y, Nagasaki T. EXAFS study of reduced ceria doped with lanthanide oxides. Solid State Ionics. 2002;**154-155**:113-118

[35] Yamazaki S, Matsui T, Ohashi T, Arita Y. Defect structures in doped CeO_2 studied by using XAFS spectrometry. Solid State Ionics. 2000;**136-137**:913-920

[36] Deguchi H, Yoshida H, Inagaki T, Horiuchi M. EXAFS study of doped ceria using multiple data set fit. Solid State Ionics. 2005;**176**:1817-1825

[37] Ohashi T, Yamazaki S, Tokunaga T, Arita Y, Matsui T, Harami T, Kobayashi K. EXAFS study of $Ce_{1-x}Gd_xO_{2-x/2}$. Solid State Ionics. 1998;**113-115**:559-564

[38] Jain P, Avila-Paredes HJ, Gapuz C, Sen S, Kim S. High-resolution 89Y and 45Sc NMR spectroscopic study of short-range structural order in Nanocrystalline Y- and Sc-doped CeO_2 and ZrO_2. The Journal of Physical Chemistry C. 2009;**113**:6553-6560

[39] Kilner JA, Waters CD. The effects of dopant cation-oxygen vacancy complexes on the anion transport properties of non-stoichiometric fluorite oxides. Solid State Ionics. 1982;**6**:253-259

[40] Rai A, Mehta P, Omar S. Ionic conduction behavior in $Sm_xNd_{0.15-x}Ce_{0.85}O_{2-\delta}$. Solid State Ionics. 2014;**263**:190-196

[41] Nowick AS, Lee WK, Jain H. Survey and interpretation of pre-exponentials of conductivity. Solid State Ionics. 1988;**28**:89-94

[42] Omar S, Wachsman ED, Nino JC. Higher conductivity Sm^{3+} and Nd^{3+} co-doped ceria-based electrolyte materials. Solid State Ionics. 2008;**178**:1890-1897

[43] Nowick AS, Wang DY, Park DS, Griffith J. Oxygen-ion conductivity and defect structure of CeO_2 doped with CaO and Y_2O_3. In: Vashishta P, Mundy JN, Shenoy GK, editors. Fast Ion Transport in Solids: Electrodes and Electrolytes. Amsterdam: Elsevier, North-Holland Publishing Co.; 1979

[44] Zhan ZL, Wen TL, Tu HY, Lu ZY. AC impedance investigation of samarium-doped ceria. Journal of the Electrochemical Society. 2001;**148**:A427-A432

[45] Kilner JA, Brook RJ. A study of oxygen ion conductivity in doped nonstoichiometric oxides. Solid State Ionics. 1982;**6**:237-252

[46] Kim DJ. Lattice-parameters, ionic conductivities, and solubility limits in fluorite-structure MO_2 oxide (M = Hf^{4+}, Zr^{4+}, Ce^{4+}, Th^{4+}, U^{4+}) solid-solutions. Journal of the American Ceramic Society. 1989;**72**:1415-1421

[47] Hong SJ, Virkar AV. Lattice-parameters and densities of rare-earth-oxide doped ceria electrolytes. Journal of the American Ceramic Society. 1995;**78**:433-439

[48] Butler V, Catlow CRA, Fender BEF, Harding JH. Dopant ion radius and ionic conductivity in cerium dioxide. Solid State Ionics. 1983;**8**:109-113

[49] Minervini L, Zacate MO, Grimes RW. Defect cluster formation in M_2O_3-doped CeO_2. Solid State Ionics. 1999;**116**:339-349

[50] Murray AD, Murch GE, Catlow CRA. A new hybrid scheme of computer simulation based on Hades and Monte Carlo: Application to ionic conductivity in Y^{3+} doped CeO_2. Solid State Ionics. 1986;**18-19**:196-202

[51] Nakayama M, Martin M. First-principles study on defect chemistry and migration of oxide ions in ceria doped with rare-earth cations. Physical Chemistry Chemical Physics. 2009;**11**:3241-3249

IntechOpen